Published in final edited form as:
Structure. 2013 March 5; 21(3): 438–448. doi:10.1016/j.str.2012.12.016.

Structural and Functional Analysis of the Regulator of G Protein Signaling 2-Gα_q Complex

Mark R. Nance[1], **Barry Kreutz**[2], **Valerie M. Tesmer**[1], **Rachel Sterne-Marr**[3], **Tohru Kozasa**[2,4], and **John J.G. Tesmer**[1,5,*]

[1]Life Sciences Institute, University of Michigan, Ann Arbor, MI 48109-2216, USA

[2]Department of Pharmacology, College of Medicine, University of Illinois, Chicago, IL 60612, USA

[3]Biology Department, Siena College, Loudonville, NY 12211, USA

[4]Laboratory of Systems Biology and Medicine, Research Center for Advanced Science and Technology, The University of Tokyo, Tokyo 153-8904, Japan

[5]Departments of Pharmacology and Biological Chemistry, University of Michigan, Ann Arbor, MI 48109, USA

SUMMARY

The heterotrimeric G protein Gα_q is a key regulator of blood pressure, and excess Gα_q signaling leads to hypertension. A specific inhibitor of Gα_q is the GTPase activating protein (GAP) known as regulator of G protein signaling 2 (RGS2). The molecular basis for how G$\alpha_{q/11}$ subunits serve as substrates for RGS proteins and how RGS2 mandates its selectivity for Gα_q is poorly understood. In crystal structures of the RGS2-Gα_q complex, RGS2 docks to Gα_q in a different orientation from that observed in RGS-G$\alpha_{i/o}$ complexes. Despite its unique pose, RGS2 maintains canonical interactions with the switch regions of Gα_q in part because its α6 helix adopts a distinct conformation. We show that RGS2 forms extensive interactions with the α-helical domain of Gα_q that contribute to binding affinity and GAP potency. RGS subfamilies that do not serve as GAPs for Gα_q are unlikely to form analogous stabilizing interactions.

INTRODUCTION

Activated G protein-coupled receptors (GPCRs) catalyze guanine nucleotide exchange on the α subunit of the heterotrimeric G protein Gαβγ. When bound to GTP, the Gα protein binds downstream effectors and thereby alters the concentration of second messengers in the cell. Signaling by Gα·GTP is controlled by the relatively slow intrinsic GTPase activity of Gα proteins, which can be accelerated via interactions with GTPase activating proteins (GAPs). GAP domains for Gα subunits are found in effector enzymes such as phospholipase C-β (PLCβ) (Chidiac and Ross, 1999; Waldo et al., 2010) and in regulator of G protein signaling (RGS) proteins. The catalytic core of RGS proteins, known as the RGS box or the RGS homology (RH) domain, consists of an oblong bundle of nine α helices (α1–α9) (Kimple et al., 2011; Tesmer, 2009). The RH domain engages all three switch regions of Gα (SwI-III) and stabilizes a transition state-like conformation for GTP hydrolysis (Tesmer et

*Correspondence: johntesmer@umich.edu.

ACCESSION NUMBERS

The PDB accession numbers for crystal forms A and B reported in this paper are 4EKC and 4EKD, respectively.

SUPPLEMENTAL INFORMATION

Supplemental Information includes two 3D molecular models and can be found with this article online at http://dx.doi.org/10.1016/j.str.2012.12.016.

al., 1997). One key residue responsible for this activity is a nearly invariant asparagine residue in the α5-α6 loop of the domain (e.g., RGS2-Asn149) (Natochin et al., 1998; Posner et al., 1999; Srinivasa et al., 1998).

There are many mechanisms that underlie the selectivity of an RGS protein for a given heterotrimeric G protein signaling pathway (Xie and Palmer, 2007). However, the selectivity of an RH domain for a given Gα subunit is strongly dictated by their specific interactions (Natochin and Artemyev, 1998). About half of the 20 RH domains from RGS proteins found in humans can bind to and serve as GAPs for Gα subunits from both the $G_{i/o}$ and $G_{q/11}$ subfamilies (such as those in the R4 subfamily, which includes RGS4), whereas some are specific for $G_{i/o}$ (such as those in the R7 subfamily, which include RGS6, -7, -9, and -11; and those in the R12 subfamily, which include RGS10, -12, and -14) (Soundararajan et al., 2008). RGS2, an R4 subfamily member, exhibits marked selectivity for $G\alpha_q$ in vitro (Heximer et al., 1997, 1999) but can serve as a GAP for $G\alpha_i$ in membrane-reconstituted systems (Cladman and Chidiac, 2002; Ingi et al., 1998). Mice lacking RGS2 have high blood pressure (Heximer et al., 2003), one of a number of observations consistent with RGS2 being a key physiological regulator of $G\alpha_q$ (Tsang et al., 2010). The inability of the RGS2 RH domain to serve as an efficient GAP for $G\alpha_{i/o}$ in vitro stems from differences in three interfacial residues that are invariant in other RGS proteins: Cys106, Asn184, and Glu191 (Ser85, Asp163, and Lys170 in rat RGS4). The C106S/N184D/E191K mutant of RGS2 (referred to hereinafter as $RGS2^{SDK}$) rescues the ability of RGS2 to serve as a GAP for $G\alpha_o$ (Heximer et al., 1999). Structural analysis shows that $RGS2^{SDK}$ binds to $G\alpha_i$ subunits in much the same way as has been observed for other RGS-$G\alpha_{i/o}$ subunit complexes (Kimple et al., 2009). Thus, it was presumed that packing incompatibilities created by RGS2-Cys106 and -Asn184 with SwI lead to loss of binding affinity for $G\alpha_{i/o}$ subunits. However, $G\alpha_q$ and $G\alpha_{i/o}$ have very similar switch regions, and it is not clear how $G\alpha_q$ tolerates the presence of Cys106 and Asn184 in RGS2. Although $RGS2^{SDK}$-Lys191 was poorly ordered in the $RGS2^{SDK}$-$G\alpha_{i/o}$ crystal structure, this position is thought to affect affinity via selective electrostatic interactions with the α-helical domain of Gα. $RGS2^{SDK}$ did not exhibit a serious binding defect with $G\alpha_q$ (Heximer et al., 1999; Kimple et al., 2009), indicating that RGS2-Cys106, -Asn184, and -Glu191 by themselves do not confer a particular ability to recognize $G\alpha_q$.

At least nine atomic structures of complexes between RGS proteins and Gα subunits have been determined (Slep et al., 2001, 2008; Soundararajan et al., 2008; Tesmer et al., 1997), all involving Gα subunits from the $G\alpha_{i/o}$ subfamily of G protein α subunits ($G\alpha_{i1}$, $G\alpha_{i3}$, $G\alpha_o$, and the $G\alpha_{t/i1}$ chimera). Thus, these structures do not provide direct insight into the molecular determinants that dictate how $G\alpha_q$ interacts with RGS proteins (in particular, RGS2). Herein, we describe two crystal structures of the RGS2 RH domain in complex with an N-terminally truncated, constitutively active mutant of $G\alpha_q$ ($^{\Delta N}G\alpha_q^{R183C}$). Compared to other RGS-$G\alpha_{i/o}$ structures, RGS2 adopts a unique orientation as it engages $G\alpha_q$ that creates more extensive inter-actions with the α-helical domain of $G\alpha_q$. The α6 helix of RGS2 is also shifted by 2–3 Å relative to other RGS domains, allowing RGS2 to maintain canonical interactions with SwIII despite its unique pose. Deleterious effects of site-directed mutation of residues in the interface of RGS2 with the α-helical domain of $G\alpha_q$ demonstrate the importance of this interface in dictating affinity and GAP potency.

RESULTS

Structural Analysis of a Complex between RGS2 and $G\alpha_q$

Although stoichiometric complexes of the RGS2 RH domain (residues 72–203) and $Mg^{2+}{\cdot}AlF_4^-$-activated $G\alpha_q$ were obtained using a number of different $G\alpha_q$ variants, we were only able to form crystals from a complex using a variant of $G\alpha_q$ in which the N-

terminal helix was deleted to reduce conformational heterogeneity, as this region is typically disordered in crystal structures of Gα in the absence of Gβγ. Our best crystals were obtained with the R183C constitutively active variant of this truncated $G\alpha_q$ ($^{\Delta N}G\alpha_q^{R183C}$). $Mg^{2+}{\cdot}AlF_4^-$-activated wild-type (WT) and R183C $G\alpha_q$ have similar affinities for RGS2, as measured via a bead-based flow cytometry binding assay (K_D = 20 ± 9 nM, n = 3, and 22 ± 9 nM, n = 3, respectively), consistent with the fact that the $G\alpha_q$-Arg183 side chain neither interacts with the RH domain nor hinders the formation of the GDP-AlF_4^- transition state. Indeed, $G\alpha_q^{R183C}$ was previously shown to be an efficient substrate for RGS proteins (Chidiac and Ross, 1999), as was the analogous R178C variant of $G\alpha_{i1}$ (Berman et al., 1996).

Initial crystals diffracted to only 7.4 Å (crystal form A, space group *C*2) but were improved by the addition of either $NiCl_2$ or $CoCl_2$, which generated a different crystal form (crystal form B, space group $P4_12_12$) that diffracted anisotropically to maximum spacings of 2.7 Å (Table 1). Initial phases for each structure were provided by molecular replacement (Figures 1A and 1B). Both crystal forms involve a hydrophobic crystal contact involving the α2 helix (SwII) and the α3-β5 loop of a 2-fold related Gα subunit. In crystal form A, a dimer interface is formed by the αB and αC helices of the α-helical domain of $G\alpha_q$ to form a four-helix bundle (Figure 1A). This contact is ablated in crystal form B due to the coordination of Co^{2+} by His105 and His109 in the αB helix (Figure 1B). The RGS2-$^{\Delta N}G\alpha_q^{R183C}$ complex from crystal form B superimposes with a root-mean-squared distance (RMSD) of 0.4 Å for 445 Cα carbons from either complex in the asymmetric unit of crystal form A, indicating that the binding of Co^{2+} does not affect the overall conformation of the complex. The RGS2-$^{\Delta N}G\alpha_q$ complex was also crystallized under the conditions of crystal form B, but these crystals diffracted poorly (anisotropic with maximum spacings of 4 Å). Although this structure was not refined to completion, it demonstrated that mutations within $G\alpha_q^{R183C}$ do not grossly affect the conformation of the complex (RMSD = 0.4 Å with RGS2-$^{\Delta N}G\alpha_q^{R183C}$).

Superposition of $G\alpha_q$ in the RGS2-$^{\Delta N}G\alpha_q^{R183C}$ complex with $G\alpha_i$ in either the RGS4-$G\alpha_{i1}$ or the $RGS2^{SDK}$-$G\alpha_{i3}$ complex reveals that the RH domain of RGS2 is rotated by 7° relative to that of RGS4 or $RGS2^{SDK}$ around an axis roughly colinear with a vector joining the $G\alpha_q$-Gly207 and Gly208 Cα carbons in SwII (Figures 1B and 1C) and passing through the backbone between $G\alpha_q$-Thr187 and Gly188 in SwI. Thr187 and Gly188 are well established as being critical for interactions with RGS proteins (Day et al., 2004; DiBello et al., 1998; Lan et al., 1998) and serve as an apparent pivot point relating WT RGS2 to $RGS2^{SDK}$ when bound to $^{\Delta N}G\alpha_q^{R183C}$ or $G\alpha_{i3}$, respectively (Figure 1C). One consequence of this rotation is that the α7 helix of the RGS2 RH domain is brought into close contact with αA and the αB-αC loop of the α-helical domain of $G\alpha_q$, a region that is structurally distinct between $G\alpha_q$ and $G\alpha_i$ subfamilies (Figures 1B and 1C). This interaction accounts for most of the additional 600 $Å^2$ of accessible surface area buried in the RGS2-$^{\Delta N}G\alpha_q^{R183C}$ complex relative to the $RGS2^{SDK}$-$G\alpha_{i3}$ complex.

Despite the distinct pose of RGS2 on $G\alpha_q$, the interactions of RGS2 with the switch regions of $G\alpha_q$ are similar to those observed in other RGS-Gα complexes, consistent with there being a conserved mechanism used by RGS proteins to accelerate GTP hydrolysis (Figures 2A and 2B). The side chain of $G\alpha_q$-Thr187 in SwI docks in a shallow, highly conserved pocket on the RH domain, $G\alpha_q$-Gln209 in SwII interacts with RGS2-Asn149, and SwIII interacts with residues at the N terminus of α6 in the RH domain, including a canonical backbone-backbone intermolecular hydrogen bond. The side chain of RGS2-Cys106 is rotated by ~35° relative to that of $RGS2^{SDK}$-Ser106, likely to help accommodate the larger size of the sulfhydryl group. We speculate that, because this group packs next to $G\alpha_q$-Thr187 (at the pivot point), it helps promote the change in the overall pose of the RGS2 RH

domain relative to that of other RGS-Gα complexes (Figures 1B and 1C). RGS2-Asn184, which also contacts $G\alpha_q$-Thr187, is conserved as an aspartic acid in other RGS proteins where it forms a specific hydrogen bond with SwI and a salt bridge with RGS2-Arg188. However, in the RGS2-$^{\Delta N}G\alpha_q^{R183C}$ complex, RGS2-Asn184 only makes van der Waals interactions with SwI and RGS2-Arg188 and thereby also likely contributes to the change in RH domain orientation. RGS2-Glu191 has been proposed to form an unfavorable electrostatic interaction with $G\alpha_i$-Glu65, thereby contributing to the selectivity of RGS2 for $G\alpha_q$ (Heximer et al., 1999). In our crystal structure, the RGS2-Glu191 side chain lacks electron density, but when modeled in a favorable extended conformation, it makes no obvious contacts with $G\alpha_q$, with the closest side chain being that of $G\alpha_q$-Arg60 (~5.0 Å away). The side chain would be at least 5.5 Å away from $G\alpha_q$-Asp71 (analogous to $G\alpha_i$-Glu65). Thus, $G\alpha_q$ may be insensitive to the identity of the amino acid found in RH domains at positions analogous to RGS2-Glu191. The tilted pose of RGS2 on $G\alpha_q$ does not occlude the binding of proteins (i.e., GRK2 and p63RhoGEF) known to form ternary complexes by interacting with the effector-binding site of $G\alpha_q$ (Shankaranarayanan et al., 2008).

RGS2 binding does not induce a significant overall conformational change in $G\alpha_q$ (Figure 3A). Indeed, previously determined structures of $G\alpha_q$ in complex with G protein-coupled receptor kinase 2 (GRK2) (Tesmer et al., 2005), p63RhoGEF (Lutz et al., 2007), and phospholipase Cβ 3 (PLCβ3) (Lyon et al., 2013; Waldo et al., 2010) superimpose similarly with that of RGS2-bound $G\alpha_q$ with an RMSD of 0.7–0.8 Å for 317 Cα atoms (0.4–0.5 Å for 270–286 Cα atoms when omitting flexible loops). However, two loops do seem to change conformation upon RGS2 binding: residues 117–127 in the αB-αC loop, which interact with the α7 helix of RGS2, and residues 242–245 in SwIII, which do not directly contact the RH domain but may alter their conformation as a consequence of the contact formed between the α6 helix of RGS2 and SwIII (Figures 2A and 2B).

Comparison of the structure of apo RGS2 (Soundararajan et al., 2008) with that of $G\alpha_q$-bound RGS2 reveals little difference in the conformation for most of the RH domain: RGS2 helices α3–8 (residues 96–192) have an RMSD of 0.65 Å for 97 Cα atoms. Residues 178–189 at the end of α7 in apo RGS2 adopt a significantly different conformation from those of $G\alpha_q$-bound RGS2 and $G\alpha_{i3}$-bound RGS2^{SDK}, likely because this region is constrained by contacts with SwI in Gα complexes (Figure 3B). Comparison of $G\alpha_q$-bound RGS2 with $G\alpha_{i3}$-bound RGS2^{SDK} reveals a significant conformational difference in the C-terminal end of the α5-α6 loop and the α6 helix of RGS2 (residues 150–171). If this region is excluded, the $G\alpha_q$ and $G\alpha_{i3}$-bound RH domains of RGS2 superimpose well, with an RMSD of 0.5 Å. The fact that the α6 helix of apo RGS2 is more similar in conformation to $G\alpha_q$-bound RGS2 than it is to $G\alpha_{i3}$-bound RGS2^{SDK} (Figure 3B) suggests that the RH domain of RGS2 has evolved a distinct conformation that complements the unique way this RH domain binds to $G\alpha_q$. In contrast, $G\alpha_{i3}$-bound RGS2^{SDK} adopts an overall conformation that is most similar to other structurally characterized R4 RGS proteins, such as RGS4. Because RGS2-Cys106, -Asn184, and -Glu191 are not directly involved in the packing of α6 within the RH domain, the conformation of the α6 region in $G\alpha_{i3}$-bound RGS2^{SDK} is probably induced by its interaction with $G\alpha_{i3}$. Notably, the α6 helix of RGS2^{SDK} is poorly ordered relative to apo RGS2 and RGS2 in complex with $^{\Delta N}G\alpha_q^{R183C}$, consistent with a nonnative conformation.

Functional Assessment of Interactions between RGS2 and $G\alpha_q$

The additional interactions formed between the RH domain of RGS2 and $G\alpha_q$ likely help promote the ability of RGS2 to serve as a GAP for $G\alpha_q$. In the interface with the α-helical domain, RGS2-Lys175, Ser179, Glu182, and Asn183 in α7 interact with $G\alpha_q$-Leu78 and Gln81 from the αA helix and $G\alpha_q$-Glu119 from the αB-αC loop (Figure 4A). Ser179 and Asn183 are unique to RGS2, whereas Leu78, Gln81, Glu119, and Lys120 are unique to $G\alpha_q$

(Figure 4B). In the SwII interface, $G\alpha_q$-Arg214 potentially makes selective interactions with the backbone in the α5-α6 loop of RGS2, as it is conserved as a shorter lysine residue in $G\alpha_{i/o}$ subunits (Figure 4B).

If these contacts are important for RGS2 function, then their disruption by site-directed mutagenesis should lead to decreased affinity and GAP potency for $G\alpha_q$. To measure relative affinity, we performed an assay in which we titrated each RGS2 variant against fluorescently labeled full-length RGS2 bound to AlF_4^--activated $G\alpha_q$ attached to beads, which were then analyzed by flow cytometry (Table 2; Figure 5A). We also measured GAP potency, which is thought to reflect indirectly the affinity of the interaction between the RGS protein and Gα subunit (Srinivasa et al., 1998), in the background of the GTPase-deficient yet RGS-responsive mutant of $G\alpha_q$, $G\alpha_q^{R183C}$ (Chidiac and Ross, 1999). WT $G\alpha_q$ cannot be assessed in this assay format because $G\alpha_q$ hydrolyzes GTP faster than it can be loaded with GTP (Chidiac et al., 1999). All RGS2 and $G\alpha_q$ variants were shown to have similar purity and concentration as determined by SDS-PAGE analysis (data not shown). Because all RGS2 mutants exhibited similar melting points to WT (Table 2), they are unlikely to exhibit major folding defects.

As anticipated, two of the most important residues from the α7 helix of RGS2 in the interface were RGS2-Asn183 and Ser179. Mutation of RGS2-Asn183 to lysine, the equivalent residue in other R4 subfamily RGS proteins, including RGS4, increased its half maximal inhibitory concentration (IC_{50}) in the binding competition assay 26-fold and its half maximal effective concentration (EC_{50}) in the GAP assay 8-fold (Figure 5; Table 2). Substitution of RGS2-Asn183 with alanine was also destabilizing, with a 5.5 fold higher IC_{50} and ~2-fold greater GAP EC_{50}. The RGS2-S179D variant exhibited 60-fold higher binding IC_{50} and 50-fold higher GAP EC_{50} (Figure 5; Table 2). Mutation of RGS2-Ser179 to asparagine, the analogous residue in RGS4 (Figure 4B), decreased potency ~2-fold in both assays. RGS2-K175 and RGS2-E182 did not appear to play a significant role in stabilizing the interface because the K175A and E182A mutations had little or no effect on $G\alpha_q$ binding or GAP potency (Table 2).

We were not able to detect as deleterious effects when interfacial residues of $G\alpha_q$ were mutated. For these experiments, variants of $G\alpha_q$ were created in the background of $G\alpha_q^{R183C}$ and evaluated for their response to RGS2 (Table 3). Our most profound effect was a surprising 3-fold lower (more potent) EC_{50} for the $G\alpha_q$-E119A/K120A mutant. $G\alpha_q$-L78V and Q81S and R214K mutations were created to change these positions into their equivalents in $G\alpha_{i/o}$ subunits (Figure 4B), but these changes had subtle or no effects on their GAP response to RGS2.

Some RGS subfamilies, such as R7 and R12, appear to be specific for $G\alpha_{i/o}$ subunits (Cho et al., 2000; Soundararajan et al., 2008). With the caveat that these RH domains may dock to $G\alpha_q$ more like RGS4 docks to $G\alpha_i$, we tested whether substitution of R7 or R12 subfamily-specific residues in the interface formed with the α-helical domain of $G\alpha_q$ could select against $G\alpha_q$ subfamily members. In support of this approach, RGS2 is a more potent GAP than RGS4 for $G\alpha_q$, with calculated EC_{50} values of 120 nM and 1.3 μM, respectively (Figure 5B; Table 2); and the RGS2-N183K and RGS2-S179N substitutions, which converted these residues to their equivalents in RGS4 (Figure 4B), individually reduced potency in both competition binding and GAP assays. However, mutation of RGS2-Asn183 to phenylalanine, which is found at this position in RGS12 and RGS14 (Figure 4B), produced a 2-fold more potent binding IC_{50} and 10-fold more potent GAP EC_{50} (Figure 5; Table 2). Conversion of RGS2-Ser179 to lysine or methionine, which are found at this position in R7 family members (Figure 4B), generated mixed results. S179K exhibited a severe defect in competition binding and in GAP response (13- and 8-fold, respectively), but

S179M was about as stabilizing as RGS2-N183F. Therefore, with the exception of the S179K mutation, the residues we tested in α7 cannot alone account for the R7 and R12 subfamily member selectivity against $G\alpha_q$ (Figure 5B; Table 2). Instead, these results indicate that the introduction of apolar side chains into the interface with the α-helical domain of $G\alpha_q$ (i.e., RGS2-S179M, -S183F, or $G\alpha_q$-E119A/K120A) generally increases affinity and GAP potency, whereas introduction of buried charge (i.e., RGS2-S179D, -S179K) is greatly destabilizing.

DISCUSSION

There can be many mechanisms for dictating the selectivity of an RGS protein for a given heterotrimeric G protein pathway, including coexpression, interactions mediated by domains other than the RH domain, and positive or negative allosteric regulation of GAP activity mediated by the Gα effector (Xie and Palmer, 2007). For example, although other RGS proteins are found in photoreceptors, RGS9-1 is required for proper termination of phototransduction by activated $G\alpha_t$. RGS9-1 is expressed only in rod and cone cells (Cowan et al., 1998); is localized to rod outer segment membranes via the interaction of its DEP domain with RGS9-1-anchoring protein (Hu et al., 2003; Martemyanov et al., 2003), which itself is expressed only in the retina (Hu and Wensel, 2002); and is most active when $G\alpha_t$ is bound to its effector target, the inhibitory subunit of cGMP phosphodiesterase (He et al., 1998). Similarly, the selectivity of RGS2 for $G\alpha_q$ in vivo can be attributed to a number of mechanisms, including a unique mode of membrane binding (Gu et al., 2007) and direct interactions with G_q-coupled receptors (Bernstein et al., 2004; Hague et al., 2005). However, the specific contacts formed between the RGS2 RH domain and Gα subunits are still undoubtedly important for dictating GAP potency and, consequently, likely determine if additional interactions are required before GAP activity can be measured (e.g., on $G\alpha_i$ subunits; Ingi et al., 1998).

The two independent crystal structures of the RGS2 RH domain in complex with $^{\Delta N}G\alpha_q^{R183C}$, one with two copies of the complex in the asymmetric unit (Figures 1A and 1B; Table 1), together demonstrate that RGS2 binds to $G\alpha_q$ in a distinct orientation from that observed in all nine other reported RGS protein complexes with $G\alpha_{i/o}$ subfamily members. Because of the distinct conformation of its α6 helical region, RGS2 retains all of the canonical interactions with the switch regions of $G\alpha_q$, despite the presence of two unique RGS2 residues (Cys106 and Asn184) that pack in the interface with SwI. These residues, along with RGS2-Glu191, prevent RGS2 from binding and serving as an efficient GAP for $G\alpha_{i/o}$ subunits (Heximer et al., 1999; Kimple et al., 2009). The ability of RGS2 to bind efficiently and serve as a GAP for $G\alpha_q$ is facilitated via an extensive contact with the α-helical domain. Substitution of residues in the interface with the α-helical domain, such as RGS2-Ser179 and -Asn183, had significant effects on binding affinity and potency of GAP activity, indicating that this interface is formed in solution and during catalysis. Influence of the α-helical domain on GAP activity has been noted for other RGS proteins, such as in the regulation of $G\alpha_t$ by RGS9 (Skiba et al., 1999). However, due to the unique tilt of RGS2 when bound to $G\alpha_q$ and the longer αB-αC loop of $G\alpha_q$, the interactions between RGS2 and the α-helical domain of $G\alpha_q$ are more extensive. The region responsible for GAP activity in the RH domain-containing effector PDZ-RhoGEF also recognizes unique features in the α-helical domain of $G\alpha_{12}$ subfamily proteins, although the RH domain of this enzyme does not directly contribute to GAP activity (Chen et al., 2008).

Without a structure of another R4 subfamily member in complex with $G\alpha_q$, we cannot directly determine if the unique orientation of $G\alpha_q$-bound RGS2 is a consequence of features unique to $G\alpha_q$. If $G\alpha_q$ is dictating the change in RH domain orientation, it would most likely be mediated by unique side chains in the three switch regions, as the backbone

atoms in $G\alpha_q$ and $G\alpha_{i/o}$ adopt very similar conformations. One such side chain is Pro185 in SwI of $G\alpha_q$, which is conserved as lysine in $G\alpha_{i/o}$ subunits. The $G\alpha_q$-P185K substitution exhibits defects in RGS2 binding (Day et al., 2004), as does the $G\alpha_i$-K180P mutation in RGS4 binding (Posner et al., 1999). These observations indicate that, in $G\alpha_q$ and $G\alpha_i$, the native residue at this position is best suited for interacting with RGS2 and RGS4, respectively, consistent with a unique pose in each complex. Other unique $G\alpha_q$ residues that could influence the pose of RGS proteins are Arg214 in SwII, Leu78 and Gln81 in the αA helix, and Glu119 and Lys120 in the αB-αC loop. However, the $G\alpha_q$-L78V, Q81S, and R214K mutations, which convert these positions to their equivalents in $G\alpha_i$, had only mild or no effect on RGS2 GAP potency. The $G\alpha_q$-E119A/K120A double mutant unexpectedly improved potency (Table 3). Therefore, of the interfacial residues unique to the $G\alpha_q$ subfamily, only $G\alpha_q$-Pro185 is a candidate for being a determinant of selectivity and perhaps docking orientation.

The balance of our data favors the hypothesis that the unique features of RGS2 are primarily responsible for its noncanonical pose when bound to $G\alpha_q$. RGS2-Cys106 and -Asn184, which are unique to RGS2, are likely the key drivers of the distinct orientation due to differences in their interactions with the side chain of $G\alpha_q$-Thr187 and the backbone of SwI (Figures 2A and 2B). RGS2-Glu191, the third uniquely conserved residue in the interface, appears too distant to form specific interactions with residues in the α-helical domain. Instead of helping dictate the unique pose, it may simply help RGS2 select against $G\alpha_{i/o}$. In addition to the importance of RGS2-Cys106 and -Asn184, our data show that residues unique to RGS2 within the α7 helix make functionally significant and likely selective interactions with the $G\alpha_q$ α-helical domain (Table 2). Finally, we note that, although the α6 region of RGS2 exhibits a unique conformation that allows RGS2 to maintain canonical interactions with SwIII of $G\alpha_q$ (Figure 3B), structural evidence suggests that this region is flexible and can accommodate binding to either $G\alpha_i$ (in the context of $RGS2^{SDK}$) or $G\alpha_q$ subunits. Therefore, we do not believe it can be the driving force for the unique pose exhibited by $G\alpha_q$-bound RGS2.

Our results provide a framework by which to interpret existing biochemical data for RGS2 and RGS4 concerning their ability to serve as GAPs for $G\alpha_{i/o}$ and $G\alpha_q$ in vitro. We predict that RGS4 binds to $G\alpha_q$ in a way that is similar to how it binds to $G\alpha_i$ but with lower potency (Figure 5B) because the interactions of RGS4 with the α-helical domain of $G\alpha_q$ are not as complementary. Similarly, conversion of RGS2 to $RGS2^{SDK}$ does not greatly affect its ability to bind to $G\alpha_q$ (Heximer et al., 1999; Kimple et al., 2009) because $RGS2^{SDK}$ docks to $G\alpha_q$ in a manner similar to RGS4, with its α6 region changing conformation to maintain interactions with SwIII (as in the $RGS2^{SDK}$-$G\alpha_{i3}$ complex; Figure 3B). However, $RGS2^{SDK}$ binds dramatically better to $G\alpha_{i/o}$ subunits than WT RGS2 because it adopts an RGS4-like pose when bound to $G\alpha_{i/o}$ (Kimple et al., 2009). In this way, $RGS2^{SDK}$ can better accommodate the side chain of $G\alpha_i$-Lys180, and the RGS2-E191K substitution creates a favorable salt bridge with $G\alpha_i$-Glu65 in the α-helical domain. Introduction of the reverse substitutions into RGS4 (i.e., S85C/D163N/K170E, or $RGS4^{CNE}$) does not enhance its potency against $G\alpha_q$ (Heximer et al., 1999). If $RGS4^{CNE}$ were to adopt an RGS2-like pose on $G\alpha_q$, we predict that this would result in less complementary interactions with the α-helical domain, consistent with the reductions in potency we noted for the RGS2-S179N and -N183K mutations that convert these positions to their equivalents in RGS4 (Table 2). There is also no evidence that the RGS4 α6 helix region is flexible enough to maintain optimal interactions with SwIII in this pose (Moy et al., 2000). Like RGS2, $RGS4^{CNE}$ fails to serve as a GAP for $G\alpha_{i/o}$ subunits in single-turnover assays (Heximer et al., 1999). This may not be due to packing “defects” with SwI, per se, but to structural incompatibilities between $G\alpha_{i/o}$ and RGS2 or $RGS4^{CNE}$ created when adopting an RGS2-like pose. Specifically, $G\alpha_i$-Lys180 in SwI could become sterically crowded by the RGS α5-α6 loop;

the $G\alpha_{i/o}$ αB-αC loop would not offer as much buried surface area and potentially introduce an electrostatic clash between $G\alpha_i$-Glu116 and $RGS4^{CNE}$-Glu161 or RGS2-Glu182; and the α6 region of these RH domains would likely collide with SwIII. The side chains of $RGS4^{CNE}$-Glu170 and RGS2-Glu191 would be ~5 Å from that of $G\alpha_i$-Glu65 in this complex. Although this potentially generates electrostatic repulsion, it seems unlikely to be a major factor in solution at physiological ionic strength, especially considering the flexibility of these residues. It remains possible that these residues are in closer proximity in a pretransition state complex (Heximer et al., 1999).

Therefore, RGS proteins that serve as efficient GAPs for both $G\alpha_q$ and $G\alpha_i$ (e.g., RGS4) are predicted to adopt an RGS4-like pose in complex with Gα while avoiding disruptive interactions with the α-helical domain. If true, then RGS proteins of the R7 and R12 subfamilies could select against $G\alpha_q$ subunits by destabilizing the interface between the α7 helix and the $G\alpha_q$ α-helical domain, as demonstrated in this study by the RGS2-S179D and -S179K substitutions. Docking RGS9, an R7 subfamily member, in an RGS4-like pose on $G\alpha_q$ predicts that RGS9-Lys397 and -Lys398 are incompatible with residues in the αA helix and αB-αC loop of $G\alpha_q$. Similarly, docking RGS10, an R12 subfamily member, suggests that RGS10-Lys131 is incompatible. Notably, all R7 and R12 subfamily members have lysine conserved at positions equivalent to RGS9-Lys397 and RGS10-Lys131, whereas most R4 members have glutamic acid at this position (e.g., RGS2-Glu182) (Figure 4B). Although loss of the interactions of RGS2-Glu182 was not destabilizing in our assays (i.e., RGS2-E182A; Table 2), a lysine at this position would likely collide with the αB-αC loop of $G\alpha_q$ and electrostatically repel $G\alpha_q$-Lys77, which is uniquely conserved in the $G\alpha_{q/11}$ subfamily (Figure 4B).

In conclusion, our structural and functional analyses indicate that RGS2 and $G\alpha_q$ have evolved a mode of interaction that is unique from other RGS protein Gα complexes, and they provide insight into how selectivity between RGS proteins and Gα subunits is achieved at the level of direct interactions between the RH domain and Gα. There has been much interest in the development of RGS-specific inhibitors as novel targets for the regulation of heterotrimeric G protein signaling cascades (Blazer et al., 2010; Kimple et al., 2011; Sjogren et al., 2010). The unique structure of the RGS2-$G\alpha_q$ complex may allow for the identification of compounds that can selectively stabilize this interaction and ultimately guide the development of novel therapeutics that selectively serve to repress $G\alpha_q$ signaling in pathological conditions such as hypertension.

EXPERIMENTAL PROCEDURES

Proteins

Residues 72–203 spanning the RH domain of RGS2 ($RGS2^{72–203}$) and its site-directed mutants were expressed using the pMalC2H10T vector in *E. coli* as maltose-binding protein fusions and purified to homogeneity as described previously (Shankaranarayanan et al., 2008). Cleavage of the fusion with tobacco etch virus (TEV) protease leaves the exogenous sequence GEFGS at the amino terminus. Site-directed mutants were introduced using QuikChange (Stratagene) and verified by sequencing over the entire reading frame.

For crystallographic analysis, N-terminal truncations of murine $G\alpha_q$ were expressed in baculovirus-infected insect cells. WT and $G\alpha_q^{R183C}$ constructs lacking the N terminus ($^{\Delta N}G\alpha_q$ and $^{\Delta N}G\alpha_q^{R183C}$) were generated by PCR amplification of nucleotides encoding residues 36–359 from the respective cDNAs with primers that created 5′ BamHI and 3′ Hind III sites. The BamHI- and Hind III-digested PCR product was subcloned into the baculovirus expression vector, pFastBacHTB, to allow expression of N-terminally hexahistidine-tagged proteins. The $^{\Delta N}G\alpha_q^{R183C}$ construct contains a six-residue

hemagglutinin tag (DVPDYA) inserted for residues 125-ENPYVD-130 (Wilson and Bourne, 1995). These proteins were purified to homogeneity essentially as described for $G\alpha_q$ (Lyon et al., 2011), except that cells were lysed by passage through an Emulsiflex C3 homogenizer at 12,000 psi, and the eluted protein was cleaved overnight by 2% w/w TEV protease in dialysis buffer (20 mM HEPES, pH 8.0, 150 mM NaCl, 50 mM guanosine diphosphate [GDP], 2 mM dithiothreitol [DTT]) to remove the hexahistidine tag.

For binding analysis by flow cytometry, murine $G\alpha_q$ (amino acids 7–359) with an N-terminal hexahistidine tag was expressed in baculovirus-infected insect cells and purified to homogeneity as previously described (Lyon et al., 2011). The RGS2 binding affinities were measured using the $G\alpha_{i/q}$ and $G\alpha_{i/q}$-R183C proteins. $G\alpha_{i/q}$ and $G\alpha_{i/q}$-R183C are chimeras of $G\alpha_q$ that contain the N-terminal helix of $G\alpha_i$ and were produced as described in Tesmer et al. (2005) and Shankaranarayanan et al. (2008), respectively.

For GAP assays, point mutants of $G\alpha_q$ were generated in the parental baculovirus transfer construct pFastBac-His_6-$G\alpha_{i/q}$ LONG R183C, which directs expression of an N-terminally His_6-tagged chimera of rat $G\alpha_{i1}$ (amino acids 1–28) fused to mouse $G\alpha_q$ (amino acids 2–359) containing the GTPase-deficient R183C mutation. $G\alpha_q$ point mutants were introduced by overlapping PCR with mutagenic primers. Each construct was confirmed by complete DNA sequencing. His_6-$G\alpha_{i/q}$ LONG R183C and the generated mutant proteins were expressed in High Five cells (Invitrogen) and purified by nickel-NTA (QIAGEN) and Mono Q (GE Healthcare) anion exchange chromatography steps at pH 8.0.

RGS2-$G\alpha_q$ Complex Formation

A 1.2 M excess of RGS272–203 was added to $^{\Delta N}G\alpha_q$ or $^{\Delta N}G\alpha_q^{R183C}$ in a solution containing 10 mM NaF, 20 μM $AlCl_3$, and 5 mM $MgCl_2$ and incubated for 30 min on ice. Excess RGS2 was removed by size exclusion chromatography (SEC) on tandem 10/300 S200 columns (GE Healthcare) in SEC buffer (20 mM HEPES, pH 8.0, 100 mM NaCl, 5 mM $MgCl_2$, 1 mM DTT, 50 μM GDP, 20 μM $AlCl_3$, 10 mM NaF). The complex was then concentrated to 5–6 mg ml^{-1}

Crystallization and Cryoprotection

Crystals were grown using hanging-drop vapor diffusion in VDX plates on siliconized glass cover slides (Hampton Research). One microliter of the RGS2-$^{\Delta N}G\alpha_q^{R183C}$ complex at 5.5 mg ml^{-1} was combined 1:1 with well solution and suspended over 1 ml of well solution. Crystal form A grew in approximately 1–2 weeks from a well solution containing 10%–20% polyethylene glycol (PEG) 3350, 200 mM NaCl, and 100 mM 2-(*N*-morpholino)ethanesulfonic acid (MES), pH 5.5, at 4°C. These crystals were needle shaped and diffracted poorly. The best crystals were grown from 17% PEG 3350. Additive Screen HT (Hampton Research) was then used to identify conditions that generated large, single needles (crystal form B), which contained either nickel or cobalt ions and grew in 1–2 days. These crystals belonged to a different space group and diffracted to higher resolution. The best crystals of RGS2-$^{\Delta N}G\alpha_q^{R183C}$ were grown from 12% PEG 8,000, 15 mM $CoCl_2$, 200 mM NaCl, and 100 mM MES 5.5. To verify that the R183C mutation or the internal hemagglutinin tag of $^{\Delta N}G\alpha_q^{R183C}$ did not change the overall conformation of the complex, we crystallized the RGS2-$^{\Delta N}G\alpha_q$ complex using well solutions containing 11% PEG 8000, 17.5 mM $CoCl_2$, 200 mM NaCl, and 100 mM MES 5.5. All crystal forms were harvested in a cryoprotectant solution containing all components of their well solution and SEC buffer plus 30% 2-methyl-2,4-pentanediol.

Data Collection, Processing, and Model Building

X-ray diffraction data were collected at the Life Sciences Collaborative Access Team (LS-CAT) beamline of the Advanced Photon Source. Reflections were integrated, merged, and scaled using HKL2000. Crystals grown with $CoCl_2$ exhibited severe anisotropy, and the most interpretable maps were generated using diffraction data that were elliptically truncated to 3.5 Å spacings along *a** and *b**, and to 2.7 Å spacings along *c** before scaling (Lodowski et al., 2003). Phases were determined using the CCP4 implementation of PHASER (Storoni et al., 2004) using structures of $G\alpha_q$ (Tesmer et al., 2005) and RGS2 (Kimple et al., 2009; Soundararajan et al., 2008) as search models. Modeling was accomplished via successive rounds of TLS and restrained refinement in REFMAC5 for crystal form B, and with only restrained refinement for crystal form A (Winn et al., 2001), and model building in either Coot or O. Refinement of crystal form A included noncrystallographic symmetry restraints for the two complexes in the asymmetric unit. Models were validated using MolProbity (Chen et al., 2010). Atomic coordinates and structure factors for crystal forms A and B are deposited with the Protein Data Bank (PDB) under the accession codes 4EKC and 4EKD, respectively. The RGS2-$^{\Delta N}G\alpha_q$ complex had unit cell constants similar to that of crystal form B ($a = b = 60.6$ Å, $c = 348$ Å) but diffracted with high mosaicity and anisotropy to maximum spacings of only 4 Å . This crystal form did not offer any additional structural information beyond that obtained for the RGS2-$^{\Delta N}G\alpha_q^{R183C}$ complex other than to confirm that substitutions in the $^{\Delta N}G\alpha_q^{R183C}$ variant did not produce major conformational differences. Therefore, this structure was not further refined.

Flow Cytometry Protein-Interaction Assays

The binding affinities for RGS2 and its point mutants and $G\alpha_q$ were measured with a flow-cytometry-based assay (Shankaranarayanan et al., 2008). Murine $G\alpha_q$ (amino acids 7–359) was biotinylated ($bG\alpha_q$) with biotinamidohexanoic acid N-hydroxysuccinimide (Sigma-Aldrich) and attached to SPHERO streptavidin-coated particles (Spherotech). Full-length RGS2 was fluorescently labeled (F-RGS2-FL) with Alexa Fluor-488 carboxylic acid, 2,3,5,6-tetrafluoro-phenyl ester, 5-isomer (Invitrogen). Binding was performed at 4°C in a buffer consisting of 20 mM HEPES, pH 8.0, 100 mM NaCl, 5 mM $MgCl_2$, 0.1% lubrol, 2 mM DTT, 1% bovine serum albumin, 10 μM GDP, 10 mM NaF, and 30 μM $AlCl_3$. A background correction was made for equivalent samples in a buffer lacking NaF and $AlCl_3$. In agreement with previous measurements, direct binding between F-RGS2-FL and $bG\alpha_q$ yielded a $K_D \pm$ SEM of 3.3 ± 0.5 nM based on three separate experiments performed in duplicate. We similarly measured the contribution of the R183C mutation to the affinity of $G\alpha_q$ for full-length RGS2 by direct binding analysis in which $G\alpha_{i/q}$ or its R183C equivalent was biotinylated and attached to beads. The affinity of truncated $RGS2^{72–203}$ and its point mutants for $G\alpha_q$ was determined by mixing F-RGS2-FL at its K_D (3 nM) with varying concentrations of unlabeled protein competitor before addition of bead-bound $bG\alpha_q$. Samples were loaded through a Hypercyt (Intellicyt Corporation) to measure the decreased bead-associated median fluorescence intensity on an Accuri C6 Flow Cytometer. At least three independent experiments of duplicate samples were analyzed by nonlinear regression using GraphPad Prism 5.0a.

Thermofluor Analysis

To establish that the site-directed mutants made in $RGS2^{72–203}$ scaffold were properly folded, their melting profiles were analyzed using the fluorescent dye 1-anilinonapthalene-8-sulfonic acid (ANS), which binds with high affinity to hydrophobic surfaces that are exposed upon protein thermal denaturation. RGS2 samples (0.2 mg ml^{-1}) were prepared in 20 mM HEPES, pH 8.0, 500 mM NaCl, 2 mM DTT, 100 mM ANS and overlayed with silicone oil. Using a Thermofluor 384-well plate reader (Johnson & Johnson), samples were heated from 15–25°C to 80°C at 1°C min^{-1} increments in continuous ramp mode. Data from

the resulting melting curves were manually truncated to only include the range over which melting occurred for more accurate automatic determination of the melting temperature by the Thermofluor Acquire software.

GAP Assays

His-G$\alpha_{i/q}$ LONG R183C proteins were loaded with [^{32}P]-γ-GTP and mixed with RGS proteins in assay buffer, and GTP hydrolysis was monitored as described (Chidiac and Ross, 1999). Data were plotted and statistical analysis was performed with GraphPad Prism 5.0.4.

Supplementary Material

Refer to Web version on PubMed Central for supplementary material.

Acknowledgments

We thank Alisa Glukhova for technical assistance with Thermofluor analysis, Michael Ragusa for his contribution to the generation of $^{\Delta N}G\alpha_q$ baculovirus constructs, Aruna Ayer (née Shankaranarayanan) for the G$\alpha_{i/q}$ protein used in flow cytometry analysis, and Roger Sunahara and Phil Wedegaertner for WT and R183C Gα_q plasmids, respectively, from which baculovirus constructs were generated. We thank Takeharu Kawano for providing the pFastBac plasmid encoding His$_6$-G$\alpha_{i/q}$ LONG R183C. This work was supported by National Institutes of Health grants HL071818 and HL086865 (to J.T.) and GM061454 and GM074001 (to T.K.) and by National Science Foundation grants MCB0315888 and MCB0744739 (to R.S.M.). This research used the DNA Sequencing Core of the Michigan Diabetes Research and Training Center, which was supported by DK20572. Use of the Advanced Photon Source was supported by the U.S. Department of Energy, Office of Science, Office of Basic Energy Sciences under Contract No. DE-AC02-06CH11357. Use of the LS-CAT Sector 21 was supported by the Michigan Economic Development Corporation and the Michigan Technology Tri-Corridor for the support of this research program (Grant 085P1000817).

References

Berman DM, Wilkie TM, Gilman AG. GAIP and RGS4 are GTPase-activating proteins for the Gi subfamily of G protein alpha subunits. Cell. 1996; 86:445–452. [PubMed: 8756726]

Bernstein LS, Ramineni S, Hague C, Cladman W, Chidiac P, Levey AI, Hepler JR. RGS2 binds directly and selectively to the M1 muscarinic acetylcholine receptor third intracellular loop to modulate Gq/11alpha signaling. J Biol Chem. 2004; 279:21248–21256. [PubMed: 14976183]

Blazer LL, Roman DL, Chung A, Larsen MJ, Greedy BM, Husbands SM, Neubig RR. Reversible, allosteric small-molecule inhibitors of regulator of G protein signaling proteins. Mol Pharmacol. 2010; 78:524–533. [PubMed: 20571077]

Chen Z, Singer WD, Danesh SM, Sternweis PC, Sprang SR. Recognition of the activated states of Galpha13 by the rgRGS domain of PDZRhoGEF. Structure. 2008; 16:1532–1543. [PubMed: 18940608]

Chen VB, Arendall WB 3rd, Headd JJ, Keedy DA, Immormino RM, Kapral GJ, Murray LW, Richardson JS, Richardson DC. MolProbity: all-atom structure validation for macromolecular crystallography. Acta Crystallogr D Biol Crystallogr. 2010; 66:12–21. [PubMed: 20057044]

Chidiac P, Ross EM. Phospholipase C-β1 directly accelerates GTP hydrolysis by Galphaq and acceleration is inhibited by Gbeta γ subunits. J Biol Chem. 1999; 274:19639–19643. [PubMed: 10391901]

Chidiac P, Markin VS, Ross EM. Kinetic control of guanine nucleotide binding to soluble Galpha(q). Biochem Pharmacol. 1999; 58:39–48. [PubMed: 10403517]

Cho H, Kozasa T, Takekoshi K, De Gunzburg J, Kehrl JH. RGS14, a GTPase-activating protein for Gialpha, attenuates Gialpha- and G13alpha-mediated signaling pathways. Mol Pharmacol. 2000; 58:569–576. [PubMed: 10953050]

Cladman W, Chidiac P. Characterization and comparison of RGS2 and RGS4 as GTPase-activating proteins for m2 muscarinic receptor-stimulated G(i). Mol Pharmacol. 2002; 62:654–659. [PubMed: 12181442]

Cowan CW, Fariss RN, Sokal I, Palczewski K, Wensel TG. High expression levels in cones of RGS9, the predominant GTPase accelerating protein of rods. Proc Natl Acad Sci USA. 1998; 95:5351–5356. [PubMed: 9560279]

Day PW, Tesmer JJ, Sterne-Marr R, Freeman LC, Benovic JL, Wedegaertner PB. Characterization of the GRK2 binding site of Galphaq. J Biol Chem. 2004; 279:53643–53652. [PubMed: 15471870]

DiBello PR, Garrison TR, Apanovitch DM, Hoffman G, Shuey DJ, Mason K, Cockett MI, Dohlman HG. Selective uncoupling of RGS action by a single point mutation in the G protein alpha-subunit. J Biol Chem. 1998; 273:5780–5784. [PubMed: 9488712]

Gu S, He J, Ho WT, Ramineni S, Thal DM, Natesh R, Tesmer JJ, Hepler JR, Heximer SP. Unique hydrophobic extension of the RGS2 amphipathic helix domain imparts increased plasma membrane binding and function relative to other RGS R4/B subfamily members. J Biol Chem. 2007; 282:33064–33075. [PubMed: 17848575]

Hague C, Bernstein LS, Ramineni S, Chen Z, Minneman KP, Hepler JR. Selective inhibition of alpha1A-adrenergic receptor signaling by RGS2 association with the receptor third intracellular loop. J Biol Chem. 2005; 280:27289–27295. [PubMed: 15917235]

He W, Cowan CW, Wensel TG. RGS9, a GTPase accelerator for phototransduction. Neuron. 1998; 20:95–102. [PubMed: 9459445]

Heximer SP, Watson N, Linder ME, Blumer KJ, Hepler JR. RGS2/G0S8 is a selective inhibitor of Gqalpha function. Proc Natl Acad Sci USA. 1997; 94:14389–14393. [PubMed: 9405622]

Heximer SP, Srinivasa SP, Bernstein LS, Bernard JL, Linder ME, Hepler JR, Blumer KJ. G protein selectivity is a determinant of RGS2 function. J Biol Chem. 1999; 274:34253–34259. [PubMed: 10567399]

Heximer SP, Knutsen RH, Sun X, Kaltenbronn KM, Rhee MH, Peng N, Oliveira-dos-Santos A, Penninger JM, Muslin AJ, Steinberg TH, et al. Hypertension and prolonged vasoconstrictor signaling in RGS2-deficient mice. J Clin Invest. 2003; 111:445–452. [PubMed: 12588882]

Hu G, Wensel TG. R9AP, a membrane anchor for the photoreceptor GTPase accelerating protein, RGS9-1. Proc Natl Acad Sci USA. 2002; 99:9755–9760. [PubMed: 12119397]

Hu G, Zhang Z, Wensel TG. Activation of RGS9-1GTPase acceleration by its membrane anchor, R9AP. J Biol Chem. 2003; 278:14550–14554. [PubMed: 12560335]

Ingi T, Krumins AM, Chidiac P, Brothers GM, Chung S, Snow BE, Barnes CA, Lanahan AA, Siderovski DP, Ross EM, et al. Dynamic regulation of RGS2 suggests a novel mechanism in G-protein signaling and neuronal plasticity. J Neurosci. 1998; 18:7178–7188. [PubMed: 9736641]

Kimple AJ, Soundararajan M, Hutsell SQ, Roos AK, Urban DJ, Setola V, Temple BR, Roth BL, Knapp S, Willard FS, Siderovski DP. Structural determinants of G-protein alpha subunit selectivity by regulator of G-protein signaling 2 (RGS2). J Biol Chem. 2009; 284:19402–19411. [PubMed: 19478087]

Kimple AJ, Bosch DE, Giguère PM, Siderovski DP. Regulators of G-protein signaling and their Gα substrates: promises and challenges in their use as drug discovery targets. Pharmacol Rev. 2011; 63:728–749. [PubMed: 21737532]

Lan KL, Sarvazyan NA, Taussig R, Mackenzie RG, DiBello PR, Dohlman HG, Neubig RR. A point mutation in Galphao and Galphai1 blocks interaction with regulator of G protein signaling proteins. J Biol Chem. 1998; 273:12794–12797. [PubMed: 9582306]

Lodowski DT, Pitcher JA, Capel WD, Lefkowitz RJ, Tesmer JJ. Keeping G proteins at bay: a complex between G protein-coupled receptor kinase 2 and Gbetagamma. Science. 2003; 300:1256–1262. [PubMed: 12764189]

Lutz S, Shankaranarayanan A, Coco C, Ridilla M, Nance MR, Vettel C, Baltus D, Evelyn CR, Neubig RR, Wieland T, Tesmer JJ. Structure of Galphaq-p63RhoGEF-RhoA complex reveals a pathway for the activation of RhoA by GPCRs. Science. 2007; 318:1923–1927. [PubMed: 18096806]

Lyon AM, Tesmer VM, Dhamsania VD, Thal DM, Gutierrez J, Chowdhury S, Suddala KC, Northup JK, Tesmer JJG. An autoinhibitory helix in the C-terminal region of phospholipase C-β mediates $G\alpha_q$ activation. Nat Struct Mol Biol. 2011; 18:999–1005. [PubMed: 21822282]

Lyon, AM.; Dutta, S.; Boguth, CA.; Skiniotis, G.; Tesmer, JJG. Full-length $G\alpha_q$-phospholipase C-β3 structure reveals interfaces of the C-terminal coiled-coil domain. Nature Struct Mol Biol. 2013. Published online February 3, 2013. http://dx.doi.org/10.1038/nsmb.2497

Martemyanov KA, Lishko PV, Calero N, Keresztes G, Sokolov M, Strissel KJ, Leskov IB, Hopp JA, Kolesnikov AV, Chen CK, et al. The DEP domain determines subcellular targeting of the GTPase activating protein RGS9 in vivo. J Neurosci. 2003; 23:10175–10181. [PubMed: 14614075]

Moy FJ, Chanda PK, Cockett MI, Edris W, Jones PG, Mason K, Semus S, Powers R. NMR structure of free RGS4 reveals an induced conformational change upon binding Galpha. Biochemistry. 2000; 39:7063–7073. [PubMed: 10852703]

Natochin M, Artemyev NO. A single mutation Asp229/Ser confers upon Gs alpha the ability to interact with regulators of G protein signaling. Biochemistry. 1998; 37:13776–13780. [PubMed: 9753466]

Natochin M, McEntaffer RL, Artemyev NO. Mutational analysis of the Asn residue essential for RGS protein binding to G-proteins. J Biol Chem. 1998; 273:6731–6735. [PubMed: 9506972]

Posner BA, Mukhopadhyay S, Tesmer JJ, Gilman AG, Ross EM. Modulation of the affinity and selectivity of RGS protein interaction with G α subunits by a conserved asparagine/serine residue. Biochemistry. 1999; 38:7773–7779. [PubMed: 10387017]

Shankaranarayanan A, Thal DM, Tesmer VM, Roman DL, Neubig RR, Kozasa T, Tesmer JJ. Assembly of high order G alpha q-effector complexes with RGS proteins. J Biol Chem. 2008; 283:34923–34934. [PubMed: 18936096]

Sjogren, B.; Blazer, LL.; Neubig, RR. Regulators of G protein signaling proteins as targets for drug discovery. In: Lunn, Charles A., editor. Progress in Molecular Biology and Translational Science, Vol 91: Membrane Proteins as Drug Targets. San Diego, CA: Academic Press; 2010. p. 81-119.

Skiba NP, Yang CS, Huang T, Bae H, Hamm HE. The α-helical domain of Galphat determines specific interaction with regulator of G protein signaling 9. J Biol Chem. 1999; 274:8770–8778. [PubMed: 10085118]

Slep KC, Kercher MA, He W, Cowan CW, Wensel TG, Sigler PB. Structural determinants for regulation of phosphodiesterase by a G protein at 2. A Nature. 2001; 409:1071–1077.

Slep KC, Kercher MA, Wieland T, Chen CK, Simon MI, Sigler PB. Molecular architecture of Galphao and the structural basis for RGS16-mediated deactivation. Proc Natl Acad Sci USA. 2008; 105:6243–6248. [PubMed: 18434540]

Soundararajan M, Willard FS, Kimple AJ, Turnbull AP, Ball LJ, Schoch GA, Gileadi C, Fedorov OY, Dowler EF, Higman VA, et al. Structural diversity in the RGS domain and its interaction with heterotrimeric G protein alpha-subunits. Proc Natl Acad Sci USA. 2008; 105:6457–6462. [PubMed: 18434541]

Srinivasa SP, Watson N, Overton MC, Blumer KJ. Mechanism of RGS4, a GTPase-activating protein for G protein alpha subunits. J Biol Chem. 1998; 273:1529–1533. [PubMed: 9430692]

Storoni LC, McCoy AJ, Read RJ. Likelihood-enhanced fast rotation functions. Acta Crystallogr D Biol Crystallogr. 2004; 60:432–438. [PubMed: 14993666]

Tesmer JJ. Structure and function of regulator of G protein signaling homology domains. Prog Mol Biol Transl Sci. 2009; 86:75–113. [PubMed: 20374714]

Tesmer JJ, Berman DM, Gilman AG, Sprang SR. Structure of RGS4 bound to AlF4—activated G(i alpha1): stabilization of the transition state for GTP hydrolysis. Cell. 1997; 89:251–261. [PubMed: 9108480]

Tesmer VM, Kawano T, Shankaranarayanan A, Kozasa T, Tesmer JJ. Snapshot of activated G proteins at the membrane: the Galphaq-GRK2-Gbetagamma complex. Science. 2005; 310:1686–1690. [PubMed: 16339447]

Tsang S, Woo AY, Zhu W, Xiao RP. Deregulation of RGS2 in cardiovascular diseases. Front Biosci (Schol Ed). 2010; 2:547–557. [PubMed: 20036967]

Waldo GL, Ricks TK, Hicks SN, Cheever ML, Kawano T, Tsuboi K, Wang X, Montell C, Kozasa T, Sondek J, Harden TK. Kinetic scaffolding mediated by a phospholipase C-beta and Gq signaling complex. Science. 2010; 330:974–980. [PubMed: 20966218]

Wilson PT, Bourne HR. Fatty acylation of alpha z. Effects of palmitoylation and myristoylation on alpha z signaling. J Biol Chem. 1995; 270:9667–9675. [PubMed: 7536745]

Winn MD, Isupov MN, Murshudov GN. Use of TLS parameters to model anisotropic displacements in macromolecular refinement. Acta Crystallogr D Biol Crystallogr. 2001; 57:122–133. [PubMed: 11134934]

Xie GX, Palmer PP. How regulators of G protein signaling achieve selective regulation. J Mol Biol. 2007; 366:349–365. [PubMed: 17173929]

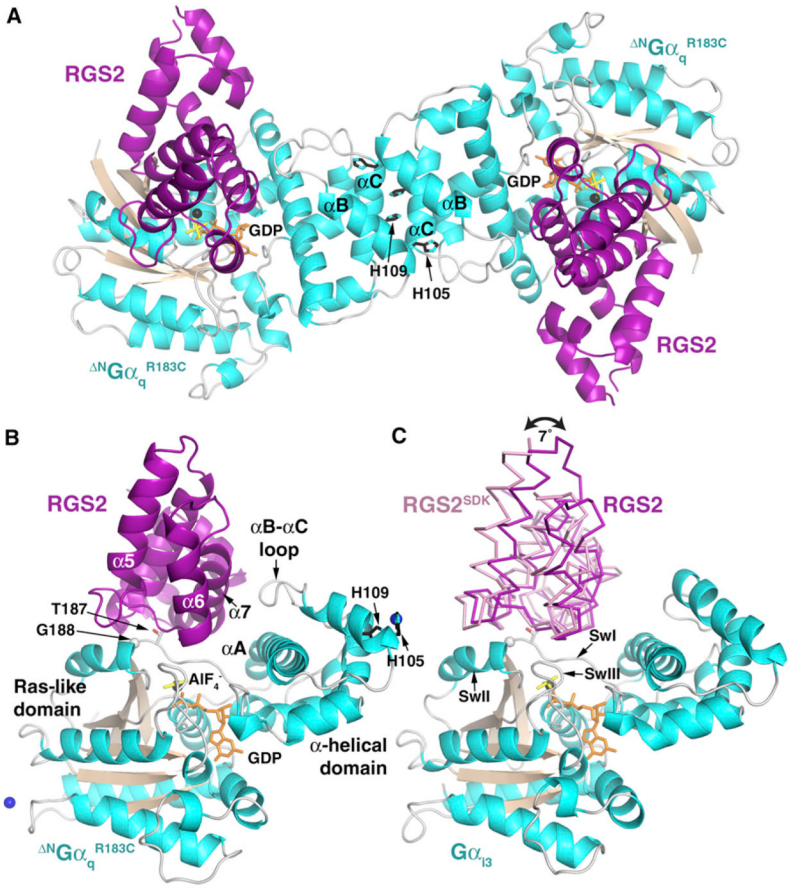

Figure 1. Structural Analysis of RGS2-Gα Subunit Complexes

(A) In crystal form A, the RGS2-$^{\Delta N}$G α_q^{R183C} complex crystallized as a dimer mediated by the αB and αC helices of the α-helical domain. The side chains of $G\alpha_q$-His105 and -His109, which coordinate Co^{2+} in crystal from B, are buried in this interface. RGS2 is shown in purple, and $G\alpha_q$ is shown with cyan helices and tan β strands. GDP and AlF_4^- are shown as orange and yellow sticks, respectively, and Mg^{2+} is shown as black spheres.

(B) The α7 helix of RGS2 makes extensive contacts with αA and the αB-αC loop of $^{\Delta N}G\alpha_q^{R183C}$. The structure shown is that of crystal form B, which was grown in the presence of Co^{2+} (blue spheres).

(C) RGS2 binds to $^{\Delta N}G\alpha_q^{R183C}$ in a different orientation than $RGS2^{SDK}$ to $G\alpha_{i3}$ (PDB code 2V4Z) (Kimple et al., 2009). RGS2 and $RGS2^{SDK}$ are shown as purple and pink ribbons, respectively. RGS2 was positioned by aligning $^{\Delta N}G\alpha_q^{R183C}$ (data not shown) with $G\alpha_{i3}$ in the 2V4Z structure. The two RH domains differ in orientation by 7°, related by an axis that passes through the peptide bond between $G\alpha_{i3}$-Thr182 and -Gly183 ($G\alpha_q$-Thr187 and -Gly188); see (B). Consequently, RGS2 is tilted toward the α-helical domain relative to $RGS2^{SDK}$, and the structurally distinct αB-αC loop of $G\alpha_{i3}$ does not come as close to α7 of the RH domain. The overall structure of RGS2 bound to $G\alpha_q$ is more similar to apo RGS2 than $RGS2^{SDK}$ bound to $G\alpha_{i3}$.

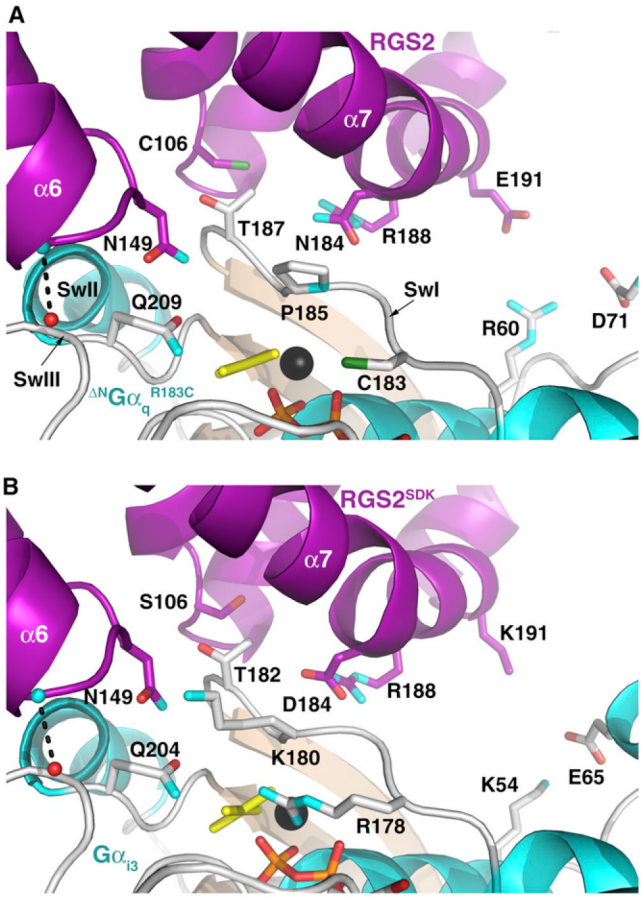

Figure 2. Unique Residues in the Interface between RGS2 and SwI of $G\alpha_q$ Likely Induce a Change in the Orientation of the RH Domain

(A) The RGS2-$^{\Delta N}G\alpha_q^{R183}$ switch region interface. As in other RGS protein complexes (see panel B), the RH domain forms canonical interactions with all three switch regions of $G\alpha_q$: Thr187 in SwI binds in a shallow pocket next to Cys106, Gln209 interacts with Asn149 in the α5-α6 loop of the RH domain, and a backbone carbonyl (red sphere)-backbone amide (cyan sphere) hydrogen bond (dashed line) is formed with SwIII. To maintain the SwIII interaction, the α6 helix region of RGS2 adopts a distinct conformation from that observed in other characterized RGS-Gα complexes. The side chain of Glu191 makes no direct interaction with $G\alpha_q$. The coloring scheme is identical to that shown in Figure 1.

(B) The RGS2^{SDK}-$G\alpha_{i3}$ switch region interface. The positions occupied by Cys106, Asn184, and Glu191 in (A) are conserved as serine, aspartate, and lysine, respectively, in other RGS proteins, as portrayed by the RGS2^{SDK} mutant. Arg178, which helps coordinate AlF_4^- (yellow sticks), corresponds to the R183C mutation shown in (A). Another prominent difference between $G\alpha_q$ and $G\alpha_{i3}$ is Pro185, see (A), and Lys180, see (B). The Lys191 side chain was partially disordered in the structure but is poised to make favorable electrostatic interactions with the side chain of $G\alpha_i$-Glu65.

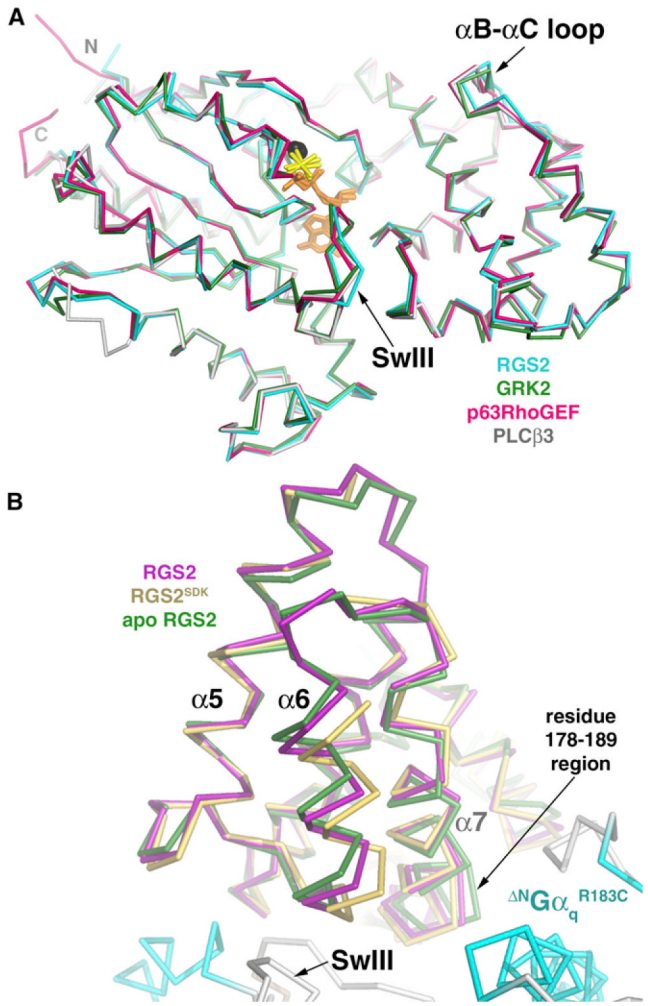

Figure 3. Conformational Differences Exhibited by $G\alpha_q$ and RGS2

(A) Cα superposition (omitting flexible loops) of AlF_4^--activated Gαq in complex with RGS2 (indicated in cyan in this study), GRK2 (green in Tesmer et al., 2005), p63RhoGEF (magenta in Lutz et al., 2007), and PLCβ3 (gray in Waldo et al., 2010). The binding of RGS2 influences the conformation of the αB-αC loop and SwIII, which exhibit structural differences among all the models.

(B) Comparison of the α6 helix region from three different structures of RGS2. $G\alpha_q$-bound RGS2 (indicated in magenta in this study) is most similar to apo RGS2 (PDB entry 2AF0; indicated in green in Soundararajan et al., 2008) in that their α6 helices adopt a distinct conformation from those of other R4 family members, as typified by the structure of $RGS2^{SDK}$ (PDB entry 2V4Z; yellow in Kimple et al., 2009). To generate this figure, the structures of apo-RGS2 and $RGS2^{SDK}$ were superimposed on $^{\Delta N}G\alpha_q{}^{R183C}$-bound RGS2, omitting the α6 region of the RH domain. The $^{\Delta N}G\alpha_q{}^{R183C}$ subunit is colored as in Figure 1.

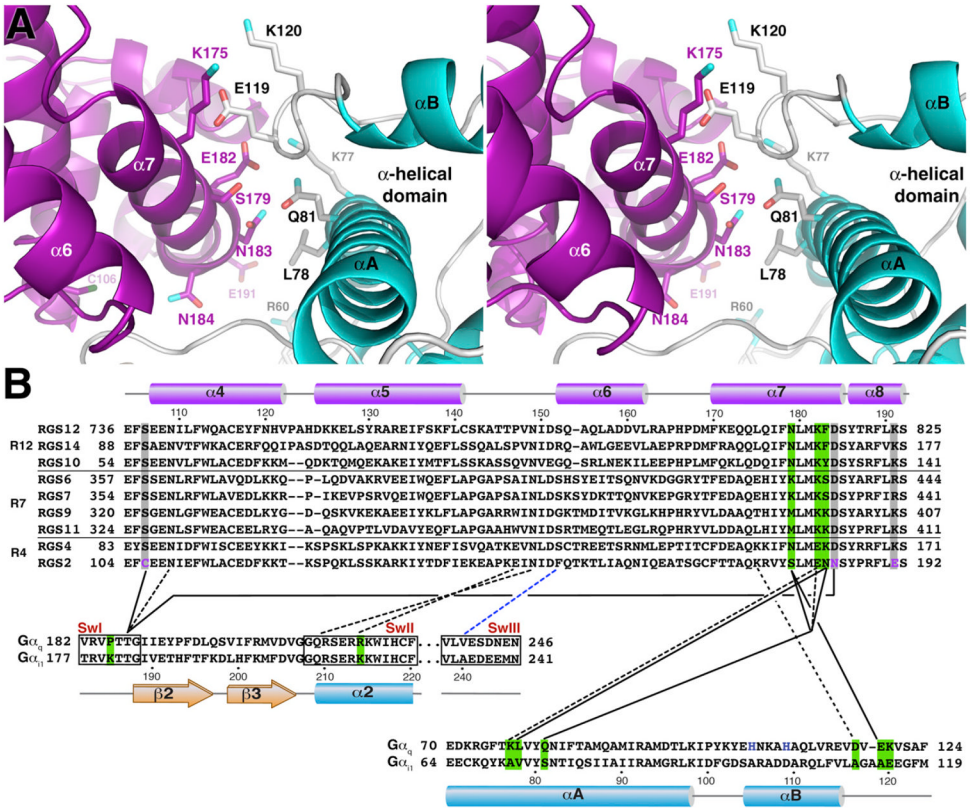

Figure 4. Contacts between Gα$_q$ and RGS2

(A) Stereo view of the interface between RGS2 and the α-helical domain of $^{\Delta N}$Gα$_q^{R183C}$, highlighting residues that were selected for site-directed mutagenesis and functional analysis. Coloring scheme is identical to that in Figure 1.

(B) Sequence conservation of interacting residues in RGS2 and Gα$_q$. Only select regions of each RH domain and Gα subunit are shown. Solid lines indicate van der Waals contacts, dashed lines indicate hydrogen bonds or salt bridges, and the blue dashed line indicates a backbone-backbone hydrogen bond. For clarity, not all intersubunit contacts are shown. Potential interactions of Glu191 are not shown because the structure predicts that its side chain will not directly interact with the α-helical domain of Gα$_q$. Grey backgrounds highlight the conservation of three contact residues that are unique to RGS2: Cys106, Asn184, and Glu191 (purple). Green highlights indicate positions that may dictate selectivity among RGS proteins or Gα$_q$/Gα$_{i/o}$ subunits. The three switch regions (SwI–III) of Gα are indicated by black boxes. The two blue positions in αB of Gα$_q$ are histidines observed to coordinate Co^{2+} in crystal form B. The secondary structure and numbering above the RH domain sequences is that of RGS2, and those below the Gα sequences are for Gα$_q$. The numbers at the beginning and end of each sequence correspond to the residue number of each individual protein sequence. All members of the R12 and R7 subfamilies are shown, but only RGS4 and RGS2 are shown for the R4 subfamily. The Swiss-Prot accession numbers for the sequences are as follows: human RGS2, P41220; rat RGS4, P49799.1; human RGS6, P49758; human RGS7, P49802; bovine RGS9, O46469; human RGS10, O43665; human RGS11, O94810; human RGS12, O14924; human RGS14, O43566; rat Gα$_{i1}$, P10824; mouse Gα$_q$, P21279.

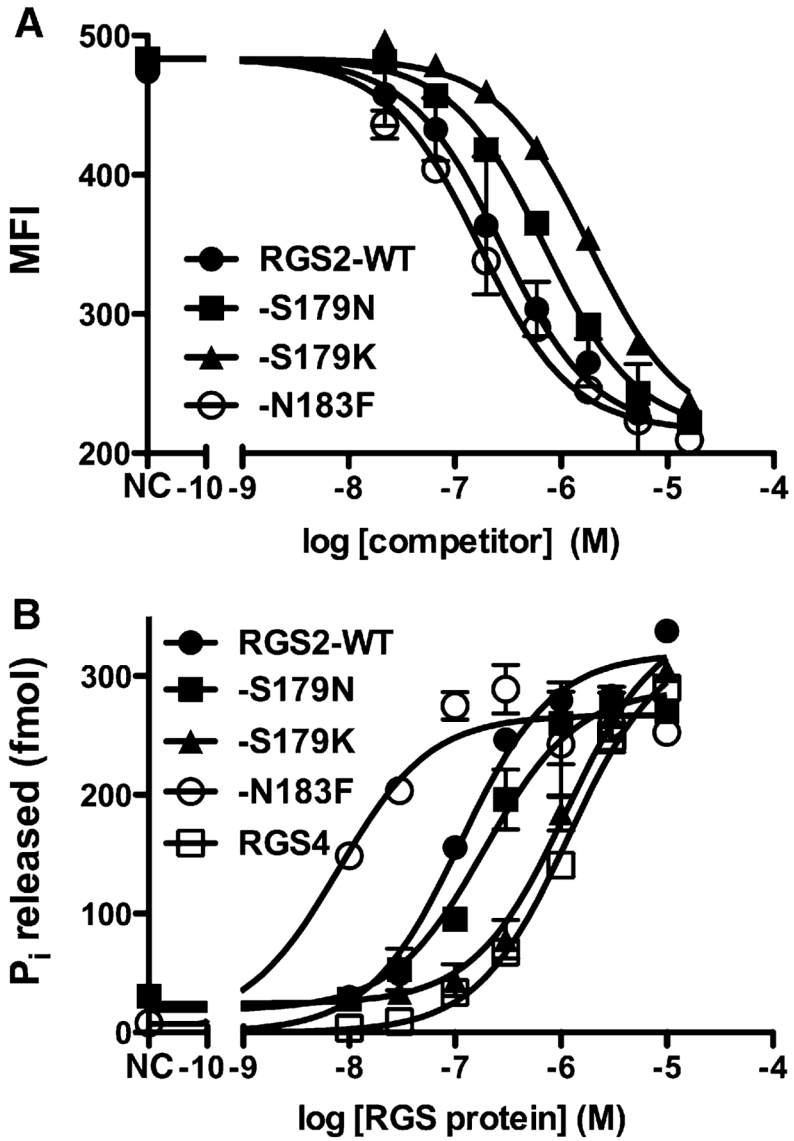

Figure 5. Biochemical Analysis of RGS2 Variants and RGS4

(A) Substitutions in RGS2 in the interface with the α-helical domain predominantly cause loss of binding affinity, as measured in a bead-based flow cytometry competition assay. Data shown are representative curves from a single experiment, with each data point measured in duplicate. Error bars correspond to the SEM. Data were fit with GraphPad Prism using a three-parameter one-site competition model with shared top and bottom values. For fitted data for all variants, see Table 2. MFI, median fluorescence intensity. NC; no competitor.

(B) Similar changes are observed in the potency of each variant for stimulating GTP hydrolysis of $G\alpha_{i/q}{}^{R183C}$. Data shown are representative curves from a single set of experiments, with each curve measured in either triplicate (RGS2-WT and RGS4) or duplicate (other variants). Error bars correspond to the SEM. Data were fit with a three-parameter one-site competition model. For fitted data for all variants, see Tables 2 and 3.

Table 1

Crystallographic Data Statistics

	Crystal Form A	**Crystal Form B ($CoCl_2$)**
X-ray Source	APS 21-ID-G	APS 21-ID-D
Wavelength (Å)	0.9786	1.0782
D_{min} (Å)	7.40 (7.53–7.40)	2.7 (2.75–2.70)
Space group	*C*2	$P4_12_12$
	a = 140	*a* = 60.2
	b = 125	*b* = 60.2
	c = 97.2	*c* = 346
	β = 124°; α = γ = 90°	α = β = γ = 90°
No. of crystals	1	1
Unique reflections	1,820 (78)	11,782 (189)
Average multiplicity	3.7 (3.7)	4.0 (2.7)
R_{sym} (%)	15.6 (51.8)	6.5 (44.1)
Completeness (%)	98.3 (100.0)	64.0 (21.4)[a]
$\langle I \rangle / \langle \sigma_I \rangle$	9.1 (2.5)	24.9 (1.6)
Refinement resolution	20.0–7.4 (7.57–7.40)	30.0–2.71 (2.78–2.71)
Total reflections used	7,811 (87)	11,078 (199)
No. of Atoms/<B Factor> (Å^2)[b]		
Protein atoms	7,318/141	3,696/111
Nonprotein atoms	74/77	66/96
Rmsds		
Bond lengths (Å)	0.007	0.008
Bond angles (°)	1.0	1.1
MolProbity Analysis		
Clashscore	18.2 (97th pctl)	10.3 (98th pctl)
Protein geometry score	2.4 (99th pctl)	2.3 (94th pctl)
Poor rotamers (%)	2.1	3.4
Cβ deviations > 0.25Å	0	0
Res. with bad bonds (%)	0	0
Res. with bad angles (%)	0	0
Ramachandran outliers (%)	0.23	0.45
Ramachandran favored (%)	93.3	94.8
R_{work} (%)	15.8 (27.1)	19.0 (33.3)
R_{free} (%)	22.0 (NA)	25.2 (37.0)
PDB Entry	4EKC	4EKD

rmsds, root-mean-square deviations; pctl, percentile; Res., residues; NA, not applicable (there were no reflections used for R_{free} in the highest resolution shell).

[a] Due to severe anisotropy of the diffraction pattern, the $CoCl_2$ data set was elliptically truncated to 3.5 Å spacings along a^* and b^*, and to 2.7 Å spacings along c^* before scaling. Overall completeness was 91.9% (92.9% in the highest resolution shell) before truncation.

[b] Includes translation/libration/screw (TLS) vibrational component.

Table 2

Characterization of RGS Domains and Their Interactions with $G\alpha_q$

RGS Variant	T_m (°)	IC_{50} in μM	Fold Increase Over WT	Log EC_{50} in nM (n)	Fold Increase Over WT
RGS2-wt	43.5 ± 0.1	0.27 ± 0.06	1	2.1 ± 0.03 (20)	1
-K175A	45.0 ± 0.4	0.56 ± 0.07	2	2.4 ± 0.03 (4)	2
-S179D	45.0 ± 0.2	16.0 ± 4	60	3.8 ± 0.26 (3)	50
-S179K	45.0 ± 0.5	3.4 ± 0.9	13	3.0 ± 0.07 (5)	8
-S179M	45.2 ± 0.1	0.13 ± 0.03	0.5	1.7 ± 0.09 (5)	0.4
-S179N	43.0 ± 0.2	0.69 ± 0.1	2.5	2.3 ± 0.06 (7)	2
-E182A	49.7 ± 0.5	0.30 ± 0.04	1	2.2 ± 0.05 (4)	1
-N183A	48.8 ± 0.2	1.5 ± 0.2	5.5	2.3 ± 0.03 (4)	2
-N183F	41.7 ± 0.1	0.17 ± 0.03	0.6	0.9 ± 0.04 (5)	0.1
-N183K	49.5 ± 0.5	7.1 ± 1	26	3.0 ± 0.03 (4)	8
RGS4-wt	–	–	–	3.1 ± 0.05 (5)	10

The melting temperatures (T_m) are derived from two separate experiments measured in triplicate. IC_{50} values ± SEM from a bead-based flow cytometry competition assay were determined from three to five experiments measured in duplicate. For EC_{50} measurements, single-turnover GTP hydrolysis by His-$G\alpha_{i/q}$ LONG R183C was measured at 20°C in the presence of various RGS constructs. Seven concentrations of each RGS protein were tested (ranging from 10 nM to 10 μM), and the resulting data were used to generate dose-response curves. The values shown represent means ± SEM of the nonlinear regression fit.

Table 3

RGS2-Mediated GAP Activity on Variants of $G\alpha_q$

$G\alpha_q$ Variant	$LogEC_{50}$ in nM (n)	Fold Increase
R183C	2.1 ± 0.03 (20)	1
R183C/L78V	2.2 ± 0.05 (9)	1
R183C/Q81S	2.4 ± 0.04 (4)	2
R183C/E119A/K120A	1.5 ± 0.06 (7)	0.3
R183C/R214K	2.0 ± 0.04 (3)	1

Single-turnover GTP hydrolysis by several variants of His-$G\alpha_{i/q}$ R183C that additionally bear the indicated mutation(s). Hydrolysis was measured at 20°C and in the presence of six concentrations of wild-type RGS2 (10 nM – 3 μM). The values shown represent means ± SEM of the nonlinear regression fit.